Three-dimensional MHD simulations of interplanetary rotational discontinuities impacting the Earth's bow shock and magnetosheath

S. Cable and Y. Lin

Department of Physics, Auburn University, Auburn, Alabama

Abstract. The first ever fully three-dimensional magnetohydrodynamic (MHD) simulations of the detailed effects of MHD discontinuities on the magnetosheath have been performed. The simulation results predict that the interaction between a rotational discontinuity (RD) and the bow shock produces an MHD wave pulse that propagates downstream from the bow shock to the magnetopause. The main components of this pulse are two slow shocks sandwiched between two time-dependent intermediate shocks; in perfectly ideal MHD, these shocks would presumably resolve into slow shocks sandwiched between two RDs. Inside the pulse, the plasma density, thermal pressure, dynamic pressure (ρv^2), and total pressure all increase, while the magnetic field magnitude decreases. The pulse convects with the downstream flow through the magnetosheath at a speed that is markedly slower than that of the original RD. It comes to rest on the magnetopause, where it raises the total pressure by as much as 75% in some locations. The pulse eventually disappears, as it is convected away by the solar wind flow around the magnetopause. The pulse remains in the magnetosheath for a few Alfvén times (i.e., solar wind Alfvén velocity divided by the Earth's radius, perhaps 1-3 min depending on the actual solar wind parameters) after the initial RD has propagated downstream past the magnetopause. Comparisons are made with previous one-dimensional and two-dimensional studies of this problem. We conclude that the pulses seen in these simulations are possible causes of magnetic impulse events observed in the ionosphere and slow mode structures observed in the inner subsolar magnetosheath.

1. Introduction

High-latitude ground magnetometers frequently record isolated large-amplitude perturbations in the Earth's magnetic field [*Lanzerotti et al.*, 1986; *Lanzerotti*, 1989; *Glassmeier et al.*, 1989]. These magnetic impulse events (MIEs) occur in conjunction with the appearance of anti-sunward moving convection vortices [*Friis-Christensen et al.*, 1988]. Observation [*Sibeck et al.*, 1989; *Farrugia et al.*, 1989; *Friis-Christensen et al.*, 1988] and theory [*Southwood and Kivelson*, 1990; *Glassmeier and Heppner*, 1992; *Lysak et al.*, 1994] generally suggest that MIEs are associated with changes in the solar wind dynamic pressure and/or interplanetary magnetic field (IMF) orientation. *Konik et al.* [1994] report that changes in the IMF orientation coincide with over 50% of observed MIEs.

The connection between MIEs and the IMF variations presumably lies in the high-latitude field lines of the Earth's magnetic field. These lines map to the outer magnetopause. Therefore if solar wind disturbances can be transmitted to the magnetopause, they can be transmitted down these field lines to high-latitude regions of the Earth's surface. *Lin et al.* [1996a,b] hypothesized that the magnetopause pressure changes that cause MIEs may be originally generated at the bow shock. In a series of one-dimensional (1-D) and two-dimensional (2-D) magnetohydrodynamic (MHD) and hybrid simulations, they showed that a sudden change in the IMF direction, i.e., a rotational discontinuity (RD), will indeed generate such pulses at the bow shock and that these pulses will then move downstream toward the magnetopause. RDs are a common feature in solar wind observations [*Neugebauer et al.*, 1984]. *Yan and Lee* [1994] obtained similar results in 2-D MHD simulations. It should be noted that another possible cause of MIEs is flux transfer events (FTEs) caused by magnetic reconnection at the magnetopause [*Saunders et al.*, 1984; *Southwood*, 1985, 1987; *Lee*, 1986]. Theory generally predicts that such events would move toward the poles under the influence of magnetic forces with speeds of about 1 km/s.

We continue the investigations of *Lin et al.* [1996a,b] into the possible link between MIEs and IMF distur-

bances by performing a fully three-dimensional MHD simulation of RDs impacting the magnetosheath. Interactions between MHD shocks and other discontinuities have been studied analytically in two dimensions [e.g., Neubauer, 1976]. The problem has been treated in the 2-D simulation studies of Yan and Lee [1994] and Lin et al. [1996b] as well as in the 1-D simulation study of Lin et al. [1996a]. We have performed the first fully three-dimensional (3-D) MHD simulations of RDs interacting with the Earth's bow shock and magnetopause. We have simulated two cases. In case 1, the RD front is set perpendicular to the Sun-Earth line, while in case 2, the RD front is aligned obliquely to the Sun-Earth line. It should be noted that kinetic effects, which cannot be included here, have been shown to be important when the bow shock changes rapidly from a parallel to a perpendicular shock. In 2-D simulations of such cases, ions reflected at the bow shock formed a pressure pulse in the foreshock [Lin et al., 1996b]. In case 1, the shock switches from quasi-perpendicular to quasi-parallel on the dusk side and from quasi-parallel to quasi-perpendicular on the dawn side. In case 2, the shock switches from quasi-parallel to quasi-perpendicular in the subsolar region.

In section 2, we describe our computational method. In section 3, we report the results of the two simulations. We summarize and discuss our results in the context of observed magnetospheric phenomena in the final section.

2. Computational Method

We model the solar wind flow around the Earth's magnetosphere with fully 3-D magnetohydrodynamic (MHD) simulations. Our code is adapted from that of Cable and Steinolfson [1995] and has also been used by Cable and Lin [1998] to study the propagation of solar wind Alfvén waves through the magnetosheath. The MHD equations are time-stepped in spherical coordinates by a two-step Lax-Wendroff method introduced by Rubin and Burstein [1967]. The use of spherical coordinates makes it a simple task to pack grid points more tightly near the magnetosphere where higher resolution is required. In this regard, our approach is similar to the steady state magnetosheath simulations of Wu [1992]. Our typical grid spacing in the region where the magnetosheath forms is about $0.075\ R_E$. At any given time, the MHD pulses that we study are resolved by four to six radial grid points. We have also performed a second simulation of one of the cases presented here (referred to as case 1) with twice the radial resolution. The results of the two different resolutions were very similar. Therefore we conclude that numerical effects have not strongly affected our results. A shock capturing term introduced by Lapidus [1967] and a small diffusive term are added to keep the simulation numerically stable. Here $\nabla \cdot \mathbf{B}$ is kept small by periodically subtracting off the contribution to $\mathbf{B}$ that possesses a

nonzero divergence. This is accomplished by use of a simple successive over-relaxation routine [Press et al., 1992].

Only the dayside of the magnetosheath is modeled, so the simulation boundaries are the magnetopause, the dawn-dusk plane (i.e., the GSE y-z plane), and a geocentric outer hemispherical shell of radius 25 R_E. The dayside magnetopause is approximated as a hard, perfectly conducting, hemispherical shell of radius 10 R_E. In the dawn-dusk plane, the fluid density ρ, pressure p, velocity $\mathbf{v}$, and the magnetic field components B_y and B_z are calculated by imposing the condition $\partial_x a = 0$, where a represents the plasma quantities just mentioned and the x axis lies along the Sun-Earth line. The magnetic field component B_x is set by requiring $\nabla \cdot \mathbf{B} = 0$. The boundary conditions on the outer boundary are discussed in section 3, in conjunction with our description of the progress of the simulation.

The simulation proceeds in two stages. First, inflow boundary conditions are imposed and fixed on the upstream boundary. The simulation runs until a steady bow shock and magnetosheath are formed in front of the magnetopause. Second, the upstream simulation data is altered to introduce an RD disturbance in the upstream solar wind. The simulation is then restarted, and the MHD disturbance is allowed to propagate through the simulation region. In this stage, the upstream boundary conditions are calculated at each time step from the analytical form of a planar RD and then updated accordingly. Strictly speaking, an RD will propagate in dissipative MHD as a time-dependent intermediate shock (TDIS). However, the resistivity of the solar wind is low enough that an RD and a TDIS will will behave very similarly.

3. Results

We present here two simulations of RDs interacting with the bow shock. In both cases, the solar wind plasma β (the ratio of thermal to magnetic pressure) is 2.0. The solar wind flows with an Alfvén Mach number of 5, which implies a sonic Mach number of 3.9. Density, pressure, and magnetic field are normalized to the upstream solar wind values ρ_0, p_0, and B_0. Velocities are normalized to the upstream Alfvén speed $v_A = B_0/\sqrt{4\pi\rho_0}$, lengths to the Earth's radius $R_E = 6370$ km, and times to the Alfvén time $t_A \equiv R_E/(B_0/\sqrt{4\pi\rho_0})$. If the solar wind density lies between 3 and 10 H^+ per cubic centimeter and the IMF strength is between 5 and 10 nT, t_A can range from 1-3 min.

3.1. Impact of a Rotational Discontinuity Aligned Perpendicular to the Sun-Earth Line

In case 1, the RD front is initially positioned perpendicular to the Sun-Earth line and placed approximately $0.4\ R_E$ upstream of the subsolar point of the bow shock. The magnetic field points along a typical Parker spiral.

The RD rotates the magnetic field about the GSE x axis by 160° clockwise as seen from the Earth. The magnetic field downstream of the RD is given by

$$B_{x0} = B_0/\sqrt{2}, \quad B_{y0} = -B_0/\sqrt{2}, \quad B_{z0} = 0, \quad (1)$$

while upstream of the RD it is given by

$$B_{x1} = \frac{B_0}{\sqrt{2}},$$
$$B_{y1} = -\frac{B_0 \cos(160°)}{\sqrt{2}}, \quad (2)$$
$$B_{z1} = \frac{B_0 \sin(160°)}{\sqrt{2}}.$$

Within the RD front, the profile of the magnetic field is given by

$$B_x(x) = \frac{B_0}{\sqrt{2}},$$
$$B_y(x) = -\frac{B_0}{\sqrt{2}} \cos(\alpha(x)), \quad (3)$$
$$B_z(x) = -\frac{B_0}{\sqrt{2}} \sin(\alpha(x)),$$

where x is the distance from Earth along the GSE x axis, and $\alpha(x)$ is the rotation angle. Here $\alpha(x)$ is given in degrees by

$$\alpha(x) = 160° \times (\frac{1}{2} + \frac{1}{2} \tanh(\frac{x - x_0}{d})),$$

where $x_0 = 13.4\ R_E$ is the perpendicular distance from the RD to the Earth (so the RD is $0.4\ R_E$ upstream of
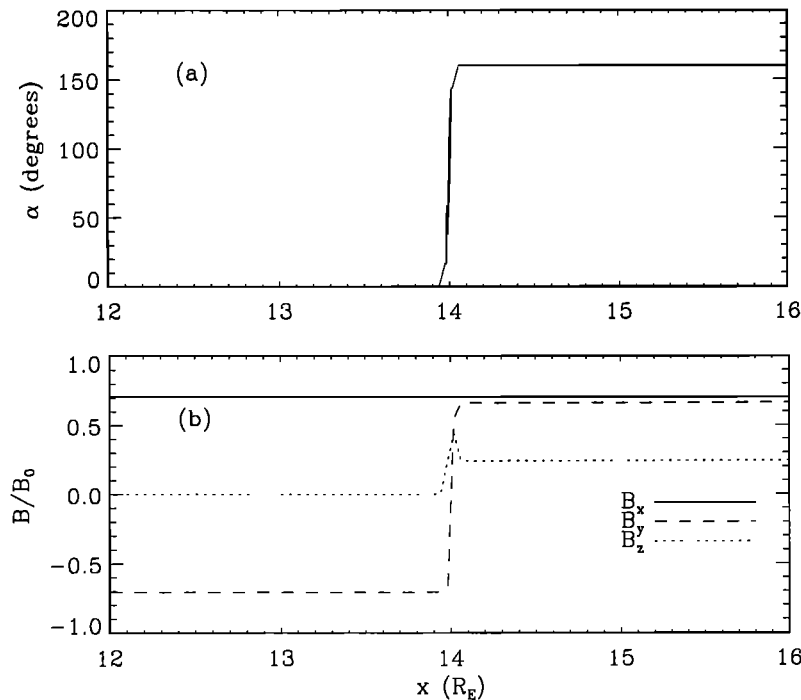
the bow shock, as mentioned above), and d is the thickness of the RD, chosen to be $0.2\ R_E$ in this case. The rotation angle $\alpha(x)$ is plotted in Figure 1a and the profiles of B_x, B_y, and B_z are plotted in Figure 1b. The perturbation in the solar wind flow is set to that required of a rotational discontinuity propagating antiparallel to the normal component of the magnetic field (i.e., propagating downstream in the simulations presented here):

$$\mathbf{v(x)} = \mathbf{v_0} + \frac{(\mathbf{B(x)} - \mathbf{B_0})}{\sqrt{4\pi\rho}},$$
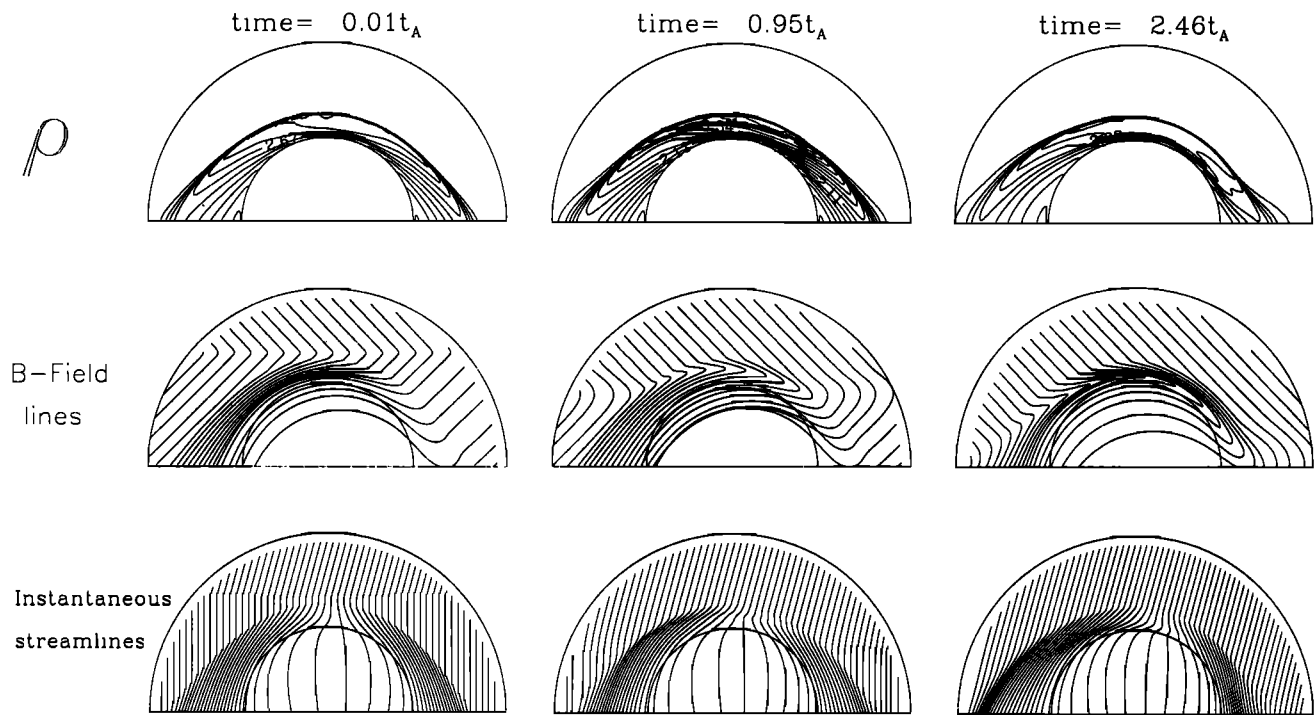
where $\mathbf{v_0}$ is the velocity downstream of the RD.

The RD propagates downstream and strikes the bow shock. The global progress of the ensuing interaction is shown in Figure 2, which displays contour plots of density in the ecliptic plane as well as traces of magnetic field lines and instantaneous streamlines projected onto the ecliptic plane, at $t = 0, 0.94t_A$, and $2.45t_A$. Dawn is on the right-side in each plot and dusk is on the left. Note that we have referred to the streamlines as "instantaneous." The streamlines do indeed indicate the direction of fluid flow at a given time but, since the flow changes with time, they do not indicate the complete path of a fluid element traveling through the simulation region. The progress of the simulation is similar in the other planes; for economy of presentation, we concentrate here on the ecliptic plane.

The original RD can be seen in the kinks in the field line traces of Figure 2 at $t = 0$. When the RD contacts the bow shock, it generates a strong pulse in pressure and density. (The first product of the interaction is actually a weak fast wave which cannot be easily seen in

Figure 1. (a) Rotation angle in degrees as a function of distance along the Sun-Earth line. The left-hand side of the graph is located at the bow shock. (b) B_x, B_y, and B_z as a function of distance along the Sun-Earth line. As in Figure 1a, the left-hand side is located at the bow shock.

time= 0.01t_A time= 0.95t_A time= 2.46t_A

ρ

B—Field lines

Instantaneous streamlines

Figure 2. Contours of density together with magnetic field lines and instantaneous streamlines in case 1 showing the evolution of the original RD and its interaction with the bow shock and magnetosheath.

Figure 2. It will be discussed in connection with Figure 3.) The pulse can be seen in Figure 2 propagating downstream toward the magnetosphere. It has significant spatial curvature, in contrast to the planar RD front. The center of the pulse lags upstream of the wings of the pulse. The curvature of the pulse increases as it propagates toward the magnetopause. By $t = 2.45t_A$, the pulse has effectively wrapped around the dayside of the magnetosphere. Note that by this time the original RD has almost completely exited the region outside of the magnetosheath, but inside the magnetosheath the pulse is still present and quite strong. We will see below that as time continues the pulse is carried downstream by the flow around the magnetopause and disappears from the dayside magnetosheath. The pulse looks similar in the noon-midnight plane with the main difference being that the density disturbance in the noon-midnight plane is largely symmetric with respect to the Sun-Earth line.
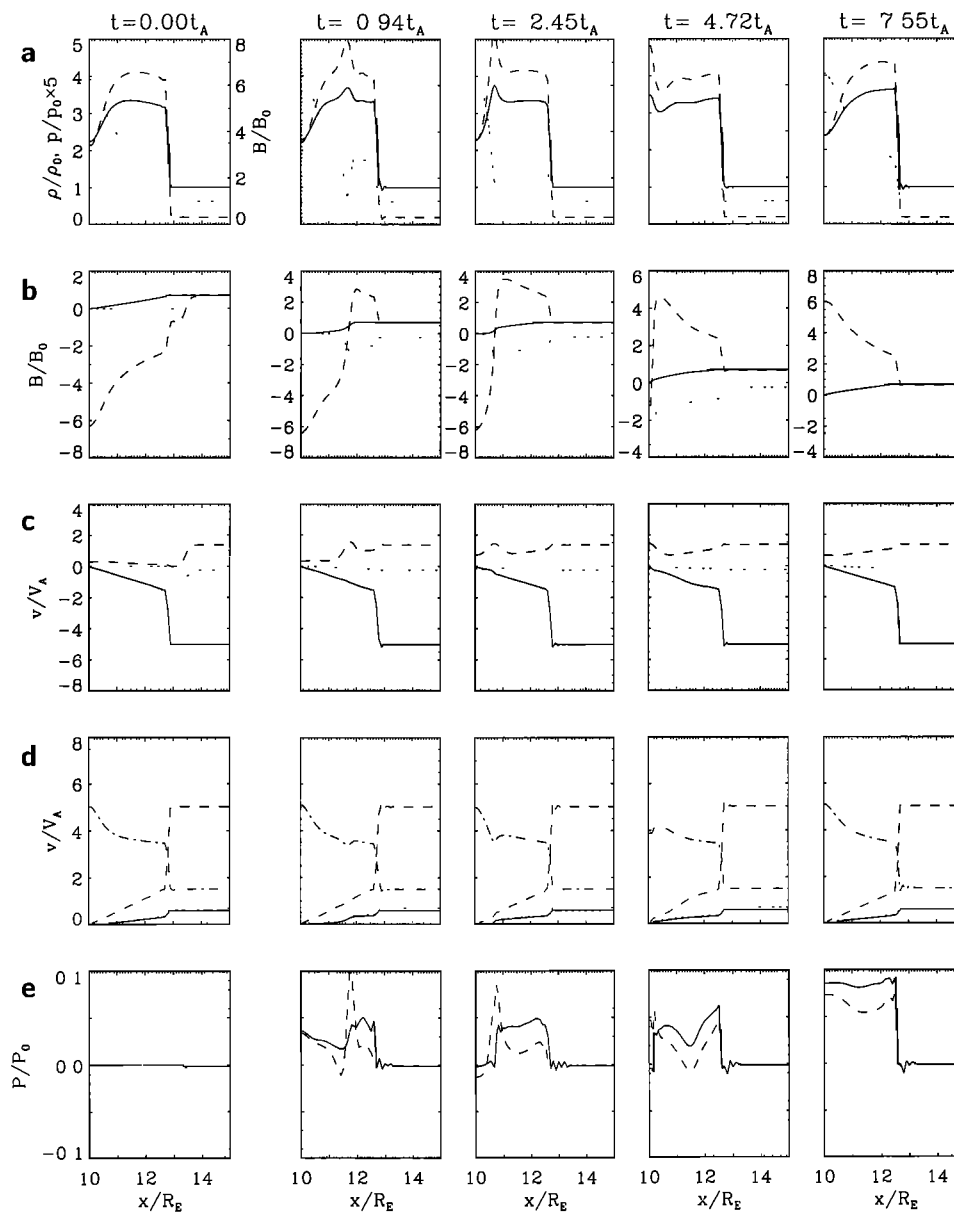
Figure 3 displays profiles of various plasma quantities along the Sun-Earth line. Figure 4 gives profiles of the same quantities along a line running radially through the ecliptic plane in the dawn region, 45° away from the Sun-Earth line. Figure 5 gives profiles of the quantities along a line running radially through the ecliptic plane in the dusk region, 45° away from the Sun-Earth line.

Figure 3 shows that the first product of the interaction is a weak fast wave. It propagates through the magnetosheath to the magnetopause in a time of about 0.63t_A, consistent with the fast wave speed in the magnetosheath. It does not show itself strongly in the per-

turbations of the plasma quantities. Its most noticeable effect is a distinct decrease in the x components of the slow and intermediate wave speeds near the magnetopause. This can been seen by comparing the wave speed plots in Figure 3 at times $t=0$ and $t = 0.94t_A$. This decrease in the wave speeds indicates that the fast wave has tilted the magnetic field lines slightly so that they are more nearly perpendicular to the Sun-Earth line.

By contrast, the pulse is seen clearly in the profiles of Figures 3–5, not only in density but also in pressure and several other quantities. In the subsolar region, the thermal pressure within the pulse rises by about 30% of the background value and the density rises by about 10%. The magnetic field magnitude decreases by 50% or more, enough to maintain approximate pressure balance within the pulse.
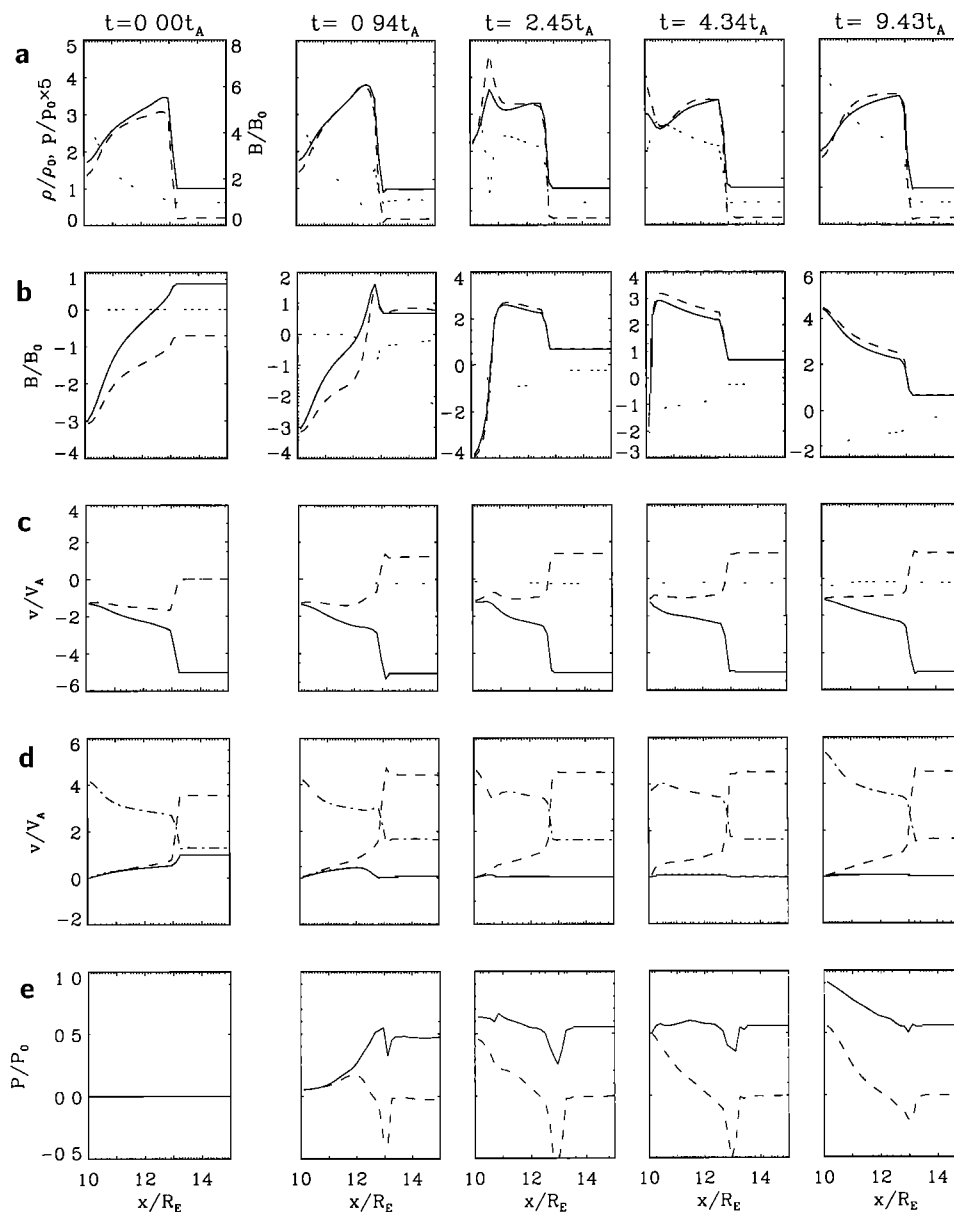
The pulse amplitude varies considerably from the dawn to dusk sectors. Figure 4 shows that in the dawn side the density in the wave increases by about 30% and the pressure by about 65%. In the subsolar region, as stated above, density increases by about 10% while the pressure increases by about 30%. In the dusk sector, however, density and pressure rise by only a few percent. This difference in behavior between the dusk side on the one hand and the dawn side and subsolar region on the other can be attributed to the distribution of B_x in the unperturbed magnetosheath. Because of magnetic field draping, B_x becomes very small in the subsolar magnetosheath near the magnetopause and actually reverses sign in the dawn magnetosheath. On the

Figure 3. Profiles of several plasma quantities in case 1 along the Sun-Earth line. (a) Density (solid line), thermal pressure (dashed line), and magnetic field magnitude (dotted line) (note that pressure values must be multiplied by 5 and that the scale for magnetic field is given on the right side of the graph). (b) B_x (solid line), B_y (dashed line), and B_z (dotted line). (c) v_x (solid line), v_y (dashed line), and v_z (dotted line). (d) r component of MHD slow wave speed (solid line), r component of MHD intermediate wave speed (dotted line), v_r (dashed line), and r component of MHD fast wave speed (dashed-dotted line) (note the r and x indicate the same direction since we are looking at profiles along the Sun-Earth line). (e) Relative change in P_r (solid line) and P_{tot} (dashed line) (P_{tot} has been calculated in a reference frame where the change in dynamic pressure across the RD is zero).

other hand, B_x is positive and of significant magnitude throughout the dusk magnetosheath. Therefore in the dusk side, the relative orientation between the pulse and the magnetic field is not too different from the relative orientation of the initial RD and the IMF. In the dawn and subsolar regions, however, the magnetic field is almost tangent to the leading surface of the pulse.

Therefore there is a much larger change in magnetic field across the pulse in the subsolar and dawn regions. (This can be seen in the field line traces in Figure 2 where kinking in the field lines is much stronger in the dawn and subsolar regions.) We can therefore expect that other plasma quantities will also be more strongly affected in the subsolar and dawn regions. From ob-
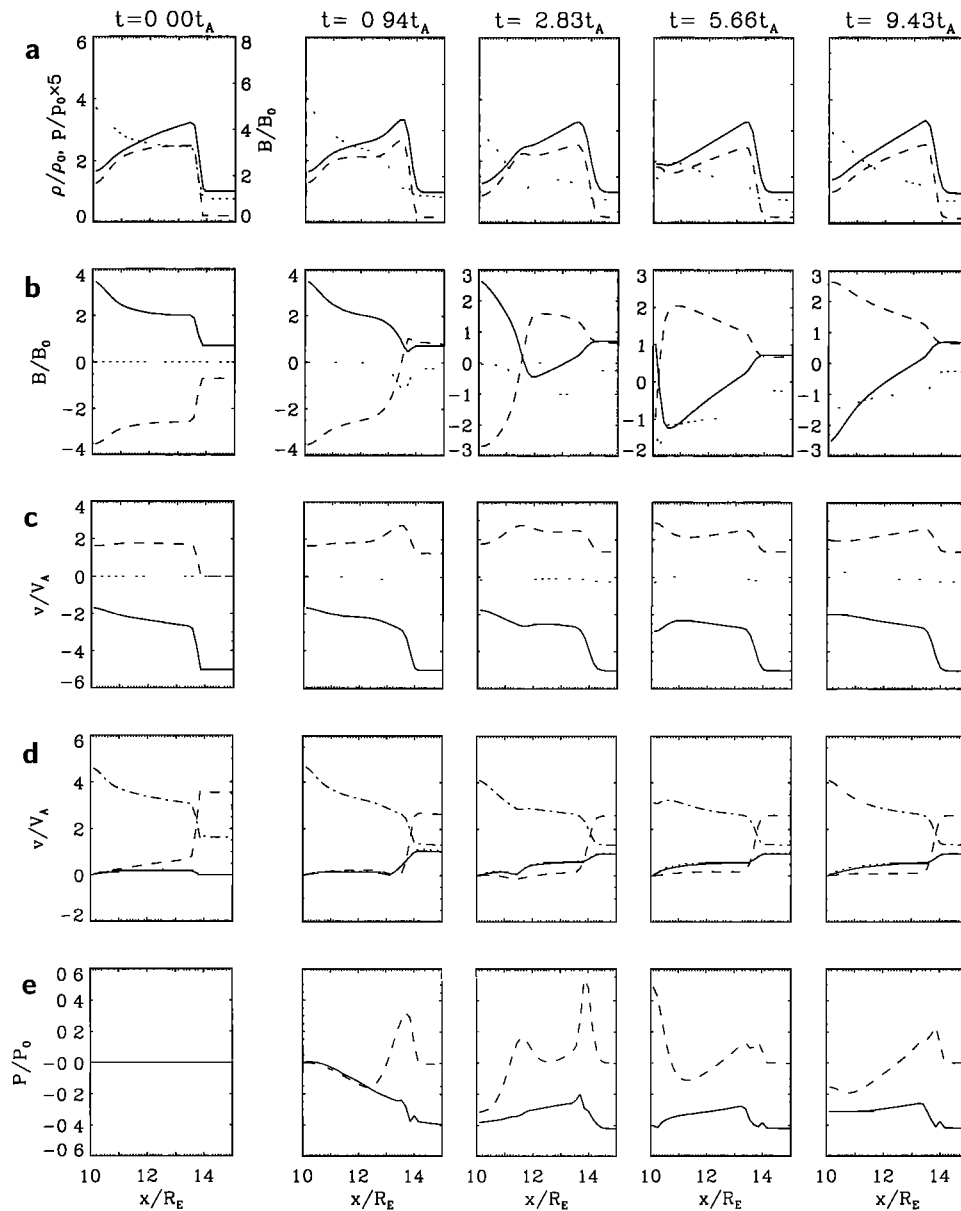
Figure 4. Profiles of several plasma quantities in case 1 along a line running through the dawn ecliptic plane, 45° away from the Sun-Earth line. (a) Density (solid line), thermal pressure (dashed line), and magnetic field magnitude (dotted line) (note that pressure values must be multiplied by 5 and that the scale for magnetic field is given on the right side of the graph). (b) B_x (solid line), B_y (dashed line), and B_z (dotted line). (c) v_x (solid line), v_y (dashed line), and v_z (dotted line). (d) r component of MHD slow wave speed (solid line), r component of MHD intermediate wave speed (dotted line), v_r (dashed line), and r component of MHD fast wave speed (dashed-dotted line). (e) Relative change in P_r (solid line) and P_{tot} (dashed line) (P_{tot} has been calculated in a reference frame where the change in dynamic pressure across the RD is zero).

servations and other simulations, it appears that the reversal of B_x on only one side of the magnetosheath leads to major differences in the propagation of Alfvén waves in the dawn and dusk magnetosheath [*Sibeck et al.*, 1997; *Cable and Lin*, 1998].

Figures 3e, 4e, and 5e show the relative changes in the total pressure $P_{tot} = \rho V^2 + p + B^2/8\pi$ and radial
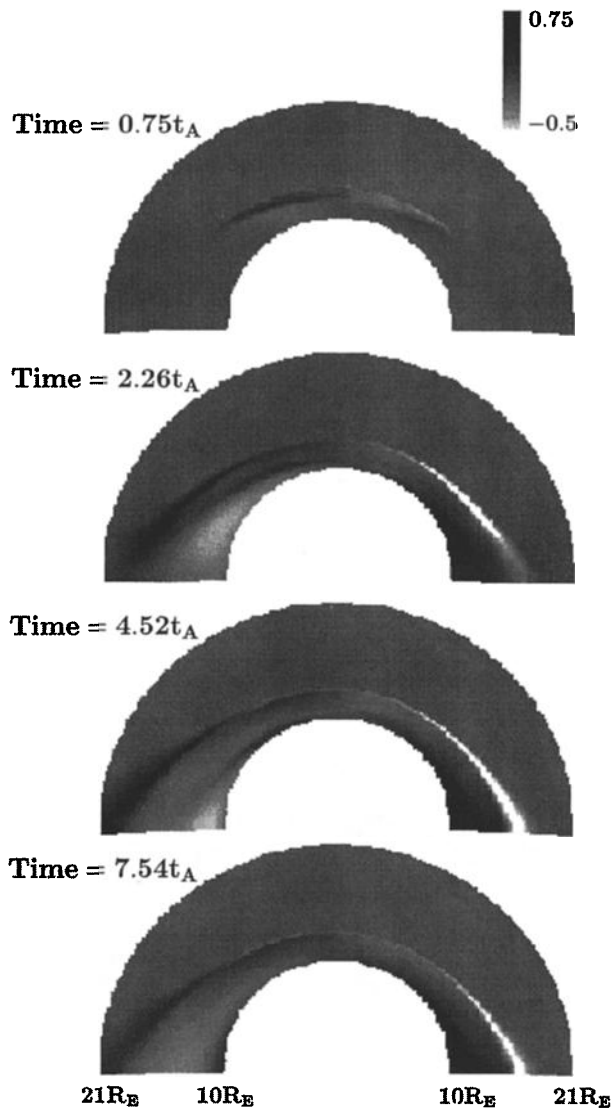
pressure $P_r = \rho V_r^2 + p + B^2/8\pi$ (where r denotes the direction heading radially outward from the Earth). In these panels, the change in total pressure has been calculated in a frame of reference where there is no change in dynamic pressure across the initial RD. This has been done to eliminate the effects of change in dynamic pressure so that the effects of change in magnetic field can

Figure 5. Profiles of several plasma quantities in case 1 along a line running through the dusk ecliptic plane, 45° away from the Sun-Earth line. (a) Density (solid line), thermal pressure (dashed line), and magnetic field magnitude (dotted line) (note that pressure values must be multiplied by 5 and that the scale for magnetic field is given on the right side of the graph). (b) B_x (solid line), B_y (dashed line), and B_z (dotted line). (c) v_x (solid line), v_y (dashed line), and v_z (dotted line). (d) r component of MHD slow wave speed (solid line), r component of MHD intermediate wave speed (dotted line), v_r (dashed line), and r component of MHD fast wave speed (dashed-dotted line). (e) Relative change in P_r (solid line) and P_{tot} (dashed line) (P_{tot} has been calculated in a reference frame where the change in dynamic pressure across the RD is zero).

be examined separately. However, note that in case 1 the two reference frames will not produce qualitatively different results, since the change in solar wind velocity across the RD is only about 20% of the background flow speed. In the subsolar region, the pulse creates in the chosen reference frame a distinct increase in P_{tot} that is 5-10% above the background pressure. The radial

pressure shows a more irregular variation of a few percent. In the dawn side, P_r and P_{tot} both increase overall by about 50%. In the final shock configuration, P_r at the magnetopause is almost 100% higher than its initial value. On the dusk side, the pulse is very distinct in P_{tot}. It rises by 60% when the pulse contacts the magnetopause and then drops about 20% below its initial
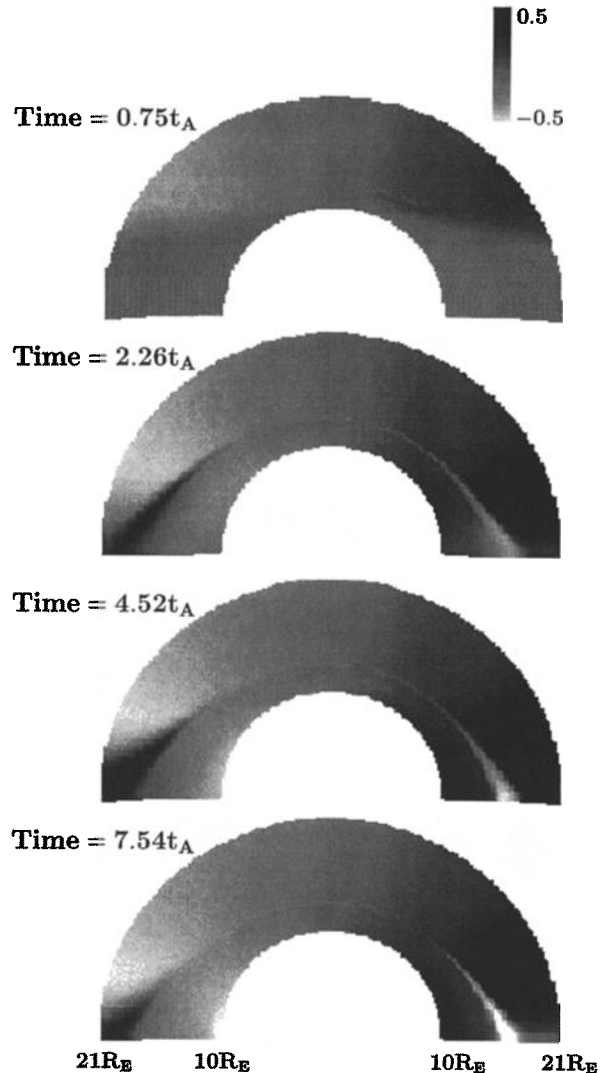
Figure 6. Gray scale plot of relative change in total pressure in the ecliptic plane for the case of the perpendicular RD at times $t = 0.75t_A$, $2.26t_A$, $4.52t_A$, and $7.54t_A$. Pressures were calculated in a frame of reference where dynamic pressure does not change across the RD, therefore the RD is not seen in the upstream solar wind.

defined on the dusk side. This contrasts with the behavior of the density and thermal pressure, which, as discussed above, change more drastically on the dawn side. This appears to be an effect of the reference frame in which the pressure is calculated. The curvature of the pulse is apparent, as in Figure 2. The pulse is in contact with the magnetopause at $t = 4.52t_A$. A new steady shock configuration has been reached by $t = 7.54t_A$. The very noticeable pressure variations near the bow shock indicate changes in the bow shock location. The change in radial pressure is smooth and even. An overall increase occurs on the dawn side, and an overall decrease occurs on the dusk side.

Approximately $4t_A$ elapses from when the pulse begins to wrap around the magnetopause (see Figure 2) until the pulse has been convected away downstream.

Figure 7. Gray scale plot of relative change in radial pressure in the ecliptic plane for the case of the perpendicular RD at times $t = 0.75t_A$, $2.26t_A$, $4.52t_A$, and $7.54t_A$.

value in the final shock configuration. P_r shows an overall drop of about 30%. Note that the deep "spikes" in the pressures around 12-14 R_E occur because the bow shock moves back from its initial position.

The relative changes in total and radial pressure are shown in the entire ecliptic plane in the gray scale plots of Figure 6 and Figure 7 respectively at times t=$0.75t_A$, $2.26t_A$, $4.52t_A$, and $7.54t_A$. As in Figures 3-4, the total pressure has been calculated in a frame of reference in which the dynamic pressure does not change across the RD. Therefore the RD does not appear in Figure 6 upstream of the bow shock. In Figure 6, the pulse is seen as an increase in total pressure. The largest increases occur on the dawn side, but the pulse form is more well

This represents a real time of 4-12 min, assuming that the solar wind density is between 3 and 10 H^+ per cubic centimeter and the IMF field strength is between 5 and 10 nT.

The 1-D MHD simulation performed by *Lin et al.* [1996a] produced a pressure pulse similar to the one described here. The pulse was made up of a combination of five MHD disturbances: a leading combination of an Earthward propagating TDIS and slow shock which raised pressure and density while lowering the magnetic field magnitude, a contact discontinuity, and a trailing combination of a Sunward propagating TDIS and slow shock which brought the pressure, density, and magnetic field magnitude back down to their undisturbed values. The thermal pressure and magnetic field varied across the pulse in such a way that the pressure $p + B^2/8\pi$ remained close to the background value. In our 3-D simulation, inhomogeneities in the plasma flow make a full analysis of wave propagation more difficult. However, the pulse we see here has all the characteristics of a slow shock/TDIS structure. Namely, as stated above, in the subsolar region, where the analogy between our work and Lin et al.'s is strongest, the pressure and magnetic field magnitude vary so that the pressure $p + B^2/8\pi$ in the pulse remains close to the background value and the quantity P_r remains relatively constant. Further, the pulse moves largely under the influence of the advecting plasma velocity. This is consistent with slow shock and TDIS motion since the slow speed in the magnetosheath is much lower than the plasma velocity. *Yan and Lee* [1994] found similar long-lived structures in their 2-D simulations of solar wind disturbances contacting a bow shock.

Finally, at about the time that the pulse strikes the magnetopause, another weak fast wave is generated at a distance of approximately 0.3 R_E upstream of the magnetopause. It propagates upstream from this point to the magnetopause in about 0.94 t_A. The sharp change in B_y in Figure 3 at the magnetopause at $t = 4.67t_A$ with a small but finite B_x indicates a large amount of magnetic tension near the magnetosphere. This fast wave may be generated in response to this tension. The magnetosheath seems to be "ringing" in response to the impact of the RD so, presumably, another fast wave will now propagate from the bow shock to the magnetopause, and the density and pressure at the bow shock will drop back closer to their previous values. However, it seems that all the important and long-lived changes in the magnetosheath have already occurred, so we have not continued the simulation beyond this point.

As stated in section 2, our code approximates the magnetopause as a hard, conducting sphere. A more complete model allowing for motion of the magnetopause will produce differences in behavior of the pulse as it approaches the magnetopause. If the pulse pushes the magnetopause in, for instance, we can expect that the pulse will remain on the magnetopause for a somewhat longer time. Consider, for example a collision between a rigid ball and a rigid wall, on the one hand, and a rigid ball and a spring on the other. The collision time between the ball and wall will be extremely small, while the collision time between the ball and spring will be finite and will depend on the spring coefficient. Further, motion of the magnetopause will make the behavior of the plasma quantities at the magnetopause more complex. For instance, magnetopause oscillations will probably cause corresponding oscillations in the density, pressure, and magnetic field of the pulse.

In addition to simulating an RD propagating along the Sun-Earth line, we have simulated RDs in the IMF represented by (1) propagating at oblique angles of 15° and 30° with respect to the Sun-Earth line. These cases each produce similar disturbances in thermal pressure, P_{tot}, and P_r along the Sun-Earth line. The main difference between the three cases is in the significant spike in v_y that appears in the leading edge of the pulse in case 1, as seen in Figure 3. This spike decreases in amplitude as the propagation direction becomes more oblique with respect to the Sun-Earth line. Presumably, this is the case because the magnetosheath plasma behind the leading edge of the pulse has a different set of upstream solar wind conditions to adjust to in these other cases than it does in case 1. In any event, the salient point is that the various pressure pulses discussed here are robust with respect to the propagation direction of the RD. Further analysis of these additional simulations will be left for future work.

3.2. Impact of a Rotational Discontinuity Aligned Obliquely to the Sun-Earth Line

In case 2, the RD changes the subsolar bow shock from a quasi-parallel shock to a quasi-perpendicular shock. We first obtain a steady state parallel shock configuration from an unperturbed magnetic field given by

$$B_{x0} = B_0, B_{y0} = 0, B_{z0} = 0.$$

The RD rotates the field to

$$B_{x1} = 0, B_{y1} = B_0, B_{z1} = 0.$$

The RD front propagates with a wave vector $\hat{k} = (-\hat{x} - \hat{y})/\sqrt{2}$. Within the front, the field is rotated about this vector by 180°. Mathematically, this is expressed by the magnetic field:

$$B_{x0}(x) = \frac{B_0}{2}(1 + \cos(\alpha(x))),$$

$$B_{y0}(x) = \frac{B_0}{2}(1 - \cos(\alpha(x))),$$

$$B_{z0}(x) = \frac{B_0}{\sqrt{2}}\sin(\alpha(x)).$$

Here $\alpha(x)$ is the rotation angle which is given in degrees by

$$\alpha(x) = 180° \times (\frac{1}{2} + \frac{1}{2}\tanh(\frac{x_0 - x \cdot \hat{k}}{d})).$$

where the RD front thickness is $d = 0.02\ R_E$ and the initial perpendicular distance from the RD to the Earth is $x_0 = 14\ R_E$. At the initial point of closest approach, the RD is separated from the dusk side of the bow shock by about $1.2\ R_E$.
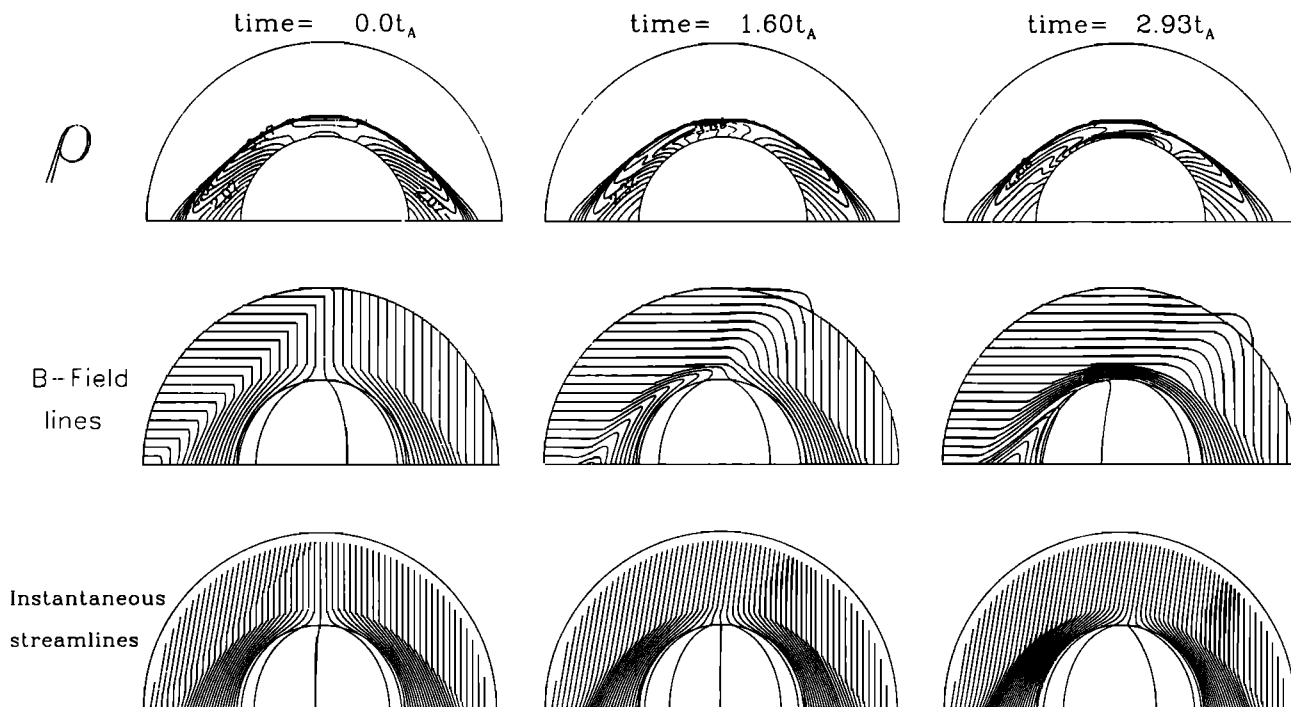
Figure 8 shows contours of density in the ecliptic plane along with field line traces and instantaneous streamlines projected into the ecliptic plane up to the time $t = 2.93t_A$. Once again, the progress of the simulation is similar in other planes, so we concentrate on the ecliptic plane. As in case 1, the pulse has significant curvature and tends to wrap around the dayside magnetopause. Note that field line kinking occurs only on the dusk side. It is absent on the dawn side because the bend in the field lines already present from field line draping is in the same general direction as the bend produced by the RD.

Figure 9, Figure 10, and Figure 11 show profiles of various plasma quantities along lines running through the subsolar region, the dawn region, and the dusk region, respectively. A pulse of high density and pressure is generated, as in the case of the perpendicular RD. The slow shock/TDIS character of this pulse is apparent in the dusk side, where the magnetic field magnitude decreases with an increase in thermal pressure. This character is not so apparent in the subsolar region, where the field strength behind the pulse is significantly higher than in front of the pulse. On the dawn side, the pulse is not clearly defined until it has contacted the magnetopause at $t = 3.49t_A$. This is largely because the line in the dawn sector along which the quantities
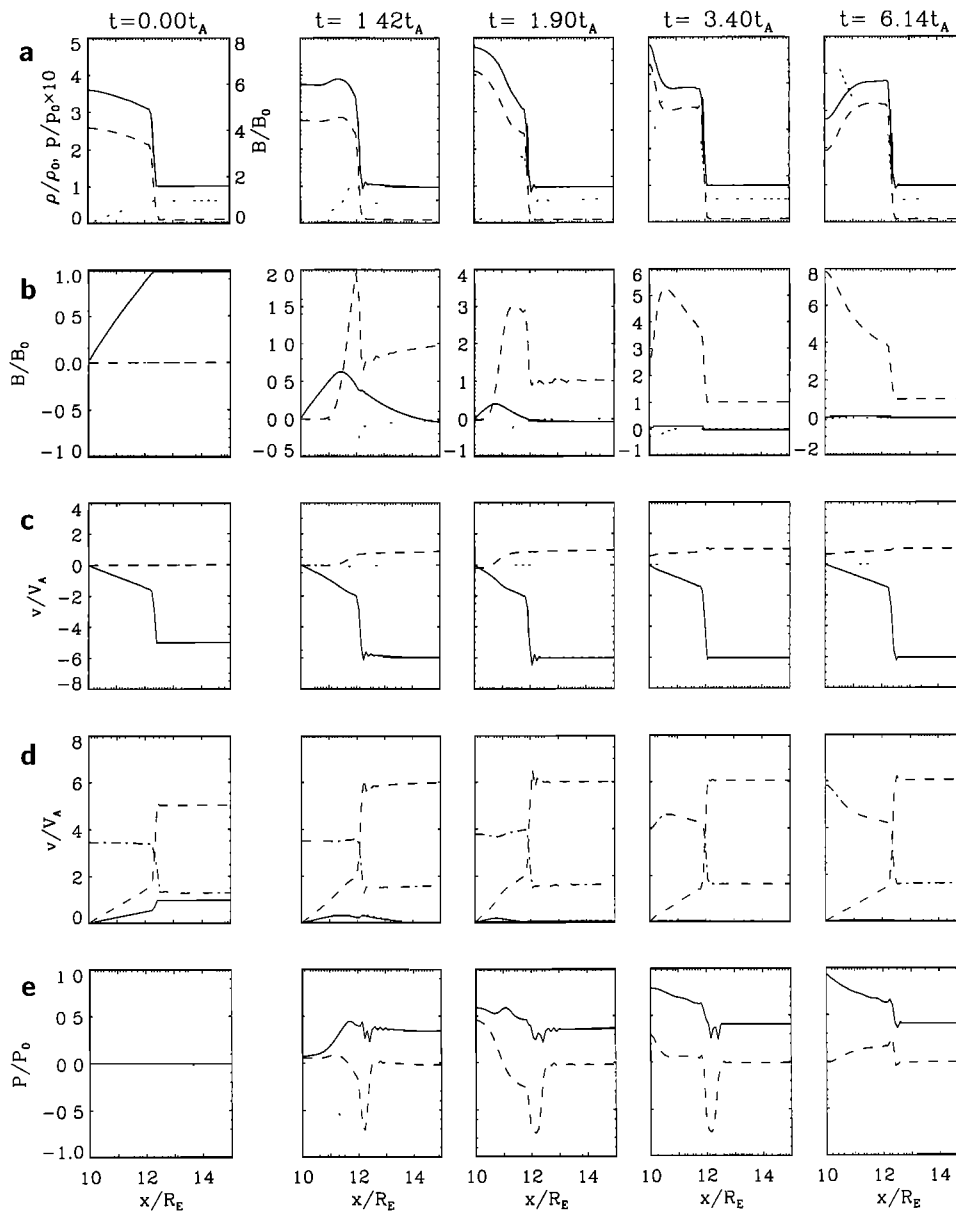
are plotted in Figure 11 cuts more nearly along the front than through it.

The pulse does not appear as well defined as it does in case 1, but its effects on the fluid quantities are just as large and, in fact, spread more evenly throughout the magnetosheath. In the subsolar region, the density increase is initially only about 15%, increasing to about 37% when the pulse actually comes into contact with the magnetopause. The thermal pressure in the pulse increases by about 26% initially and by 60% when the pulses reaches the magnetopause. On the dawn side, the pulse is barely discernible in density, as discussed above, until it contacts the magnetopause. At that point, it raises the density by about 40%. The pressure rises steadily by about 66%. On the dusk side, the density rises by about 10% and the pressure by about 25%. However, it should be noted that depletions in density and thermal pressure follow the pulse in the dusk side. At time $t = 3.49t_A$, when the pulse is in contact with the magnetopause, the drop in density from the magnetopause to the bottom of the density depletion is about 15% and the drop in pressure is about 30%.

Figures 9e, 10e, and 11e represent the relative changes in total and radial pressure, P_{tot} and P_r. As in the case of the perpendicular RD, P_{tot} is calculated in a frame of reference where the dynamic pressure does not change across the RD. In the subsolar region, the radial pressure increases by almost 100%. The total pressure at the magnetopause goes through a 50% increase and then drops back to close to its initial value. In the dawn region, P_r increases smoothly to over 100% of its orig-

Figure 8. Contours of density together with magnetic field lines and instantaneous streamlines in case 2 showing the evolution of the original RD and its interaction with the bow shock and magnetosheath.
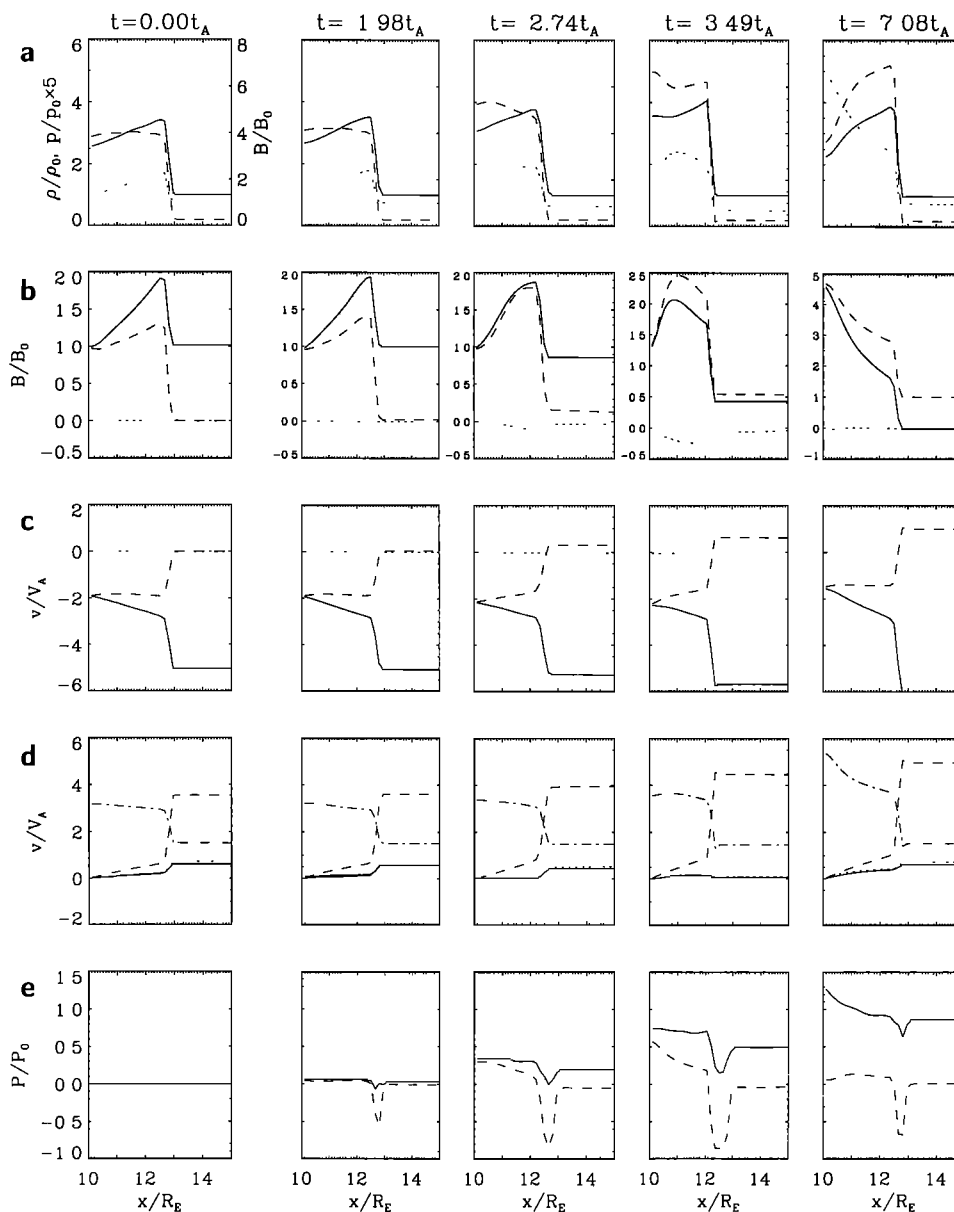
Figure 9. Profiles of several plasma quantities in case 2 along the Sun-Earth line. (a) Density (solid line), thermal pressure (dashed line), and magnetic field magnitude (dotted line) (note that pressure values must be multiplied by 10 and that the scale for magnetic field is given on the right side of the graph). (b) B_x (solid line), B_y (dashed line), and B_z (dotted line). (c) v_x (solid line), v_y (dashed line), and v_z (dotted line). (d) r component of MHD slow wave speed (solid line), r component of MHD intermediate wave speed (dotted line), v_r (dashed line), and r component of MHD fast wave speed (dashed-dotted line) (note the r and x indicate the same direction since we are looking at profiles along the Sun-Earth line). (e) Relative change in P_r (solid line) and P_{tot} (dashed line) (P_{tot} has been calculated in a reference frame where the change in dynamic pressure across the RD is zero).

inal value. P_{tot} increases by 50% at the magnetopause and then drops back to close to its original value. In the magnetopause frame of reference, P_{tot} actually increases by 75%. In the dusk region, P_r plateaus at a rise of approximately 20% before reaching its final increase of about 40%. P_{tot} at the magnetopause rises and falls by about 10% of its initial value. As in case 1, the "spikes" in the pressures around 12-14 R_E indicate that the bow shock has moved from its initial position.

Gray scale plots of the relative pressure changes in the entire ecliptic plane are shown in Figure 12 and in Figure 13. Note that the pulse appears on the dusk side as an area of decreased total pressure. As in the case of the perpendicular RD, the light and dark bands near the bow shock indicate bow shock motion.

Approximately $5t_A$ elapses from when the pulse begins to wrap around the magnetopause (see Figure 2) until the pulse has been convected away downstream,
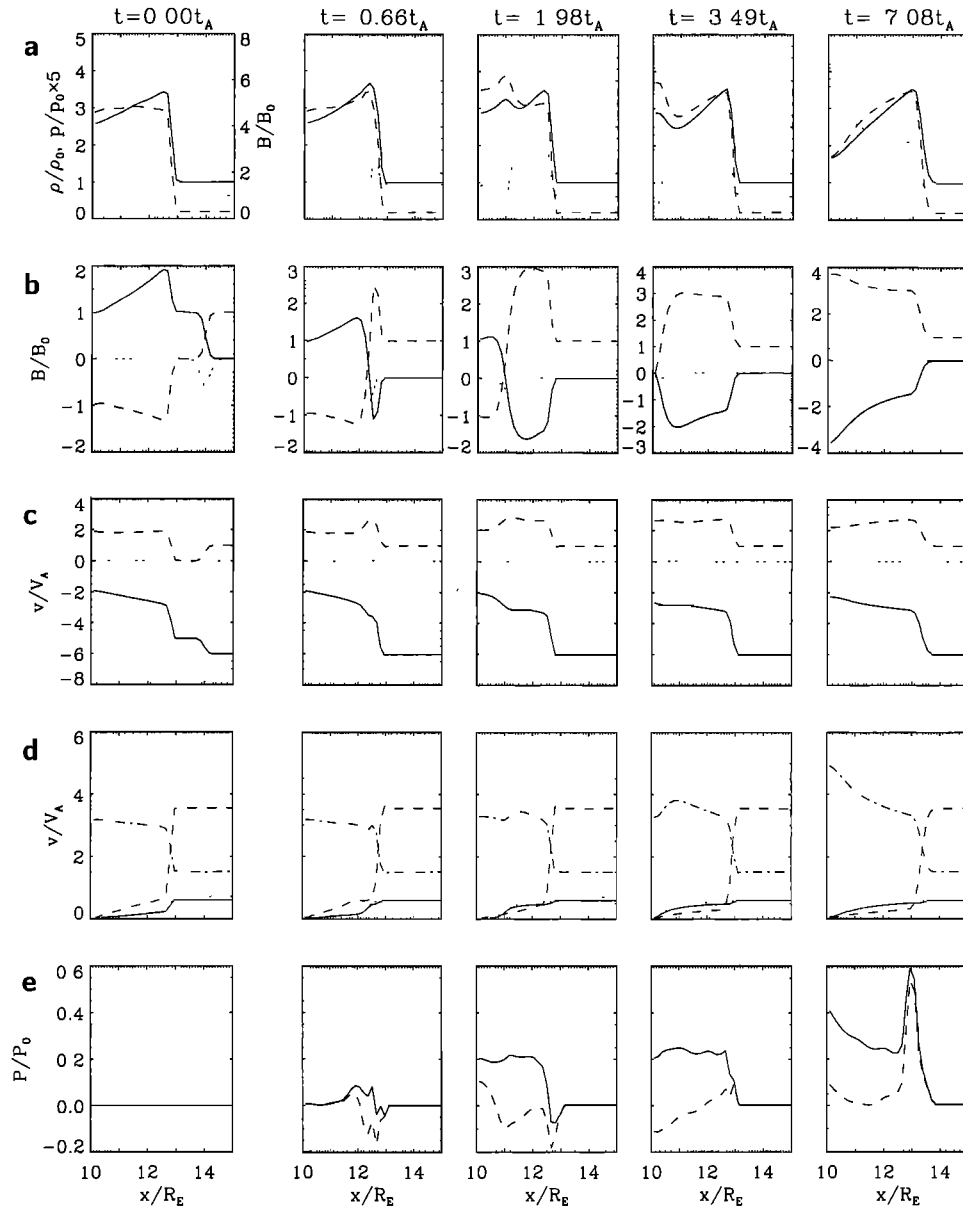
Figure 10. Profiles of several plasma quantities in case 2 along a line running through the dawn ecliptic plane, 45° away from the Sun-Earth line. (a) Density (solid line), thermal pressure (dashed line), and magnetic field magnitude (dotted line) (note that pressure values must be multiplied by 5 and that the scale for magnetic field is given on the right side of the graph). (b) B_x (solid line), B_y (dashed line), and B_z (dotted line). (c) v_x (solid line), v_y (dashed line), and v_z (dotted line). (d) r component of MHD slow wave speed (solid line), r component of MHD intermediate wave speed (dotted line), v_r (dashed line), and r component of MHD fast wave speed (dashed-dotted line). (e) relative change in P_r (solid line) and P_{tot} (dashed line) (P_{tot} has been calculated in a reference frame where the change in dynamic pressure across the RD is zero).

similar to the time found for case 1. This represents a real time of 5-15 min, assuming the same possible range of solar wind parameters.

4. Summary and Discussion

We have simulated two cases of interplanetary RDs interacting with the Earth's bow shock. In case 1, the unperturbed magnetic field points along a Parker spiral, and the RD front is perpendicular to the Sun-Earth line. In case 2, the unperturbed magnetic field points in the GSE x direction, and the RD front is aligned obliquely to the Sun-Earth line. The interactions produce strong pressure pulses that raise density and pressure by several tens of percent. The pulses move downstream in the magnetosheath, come to rest on the magnetopause
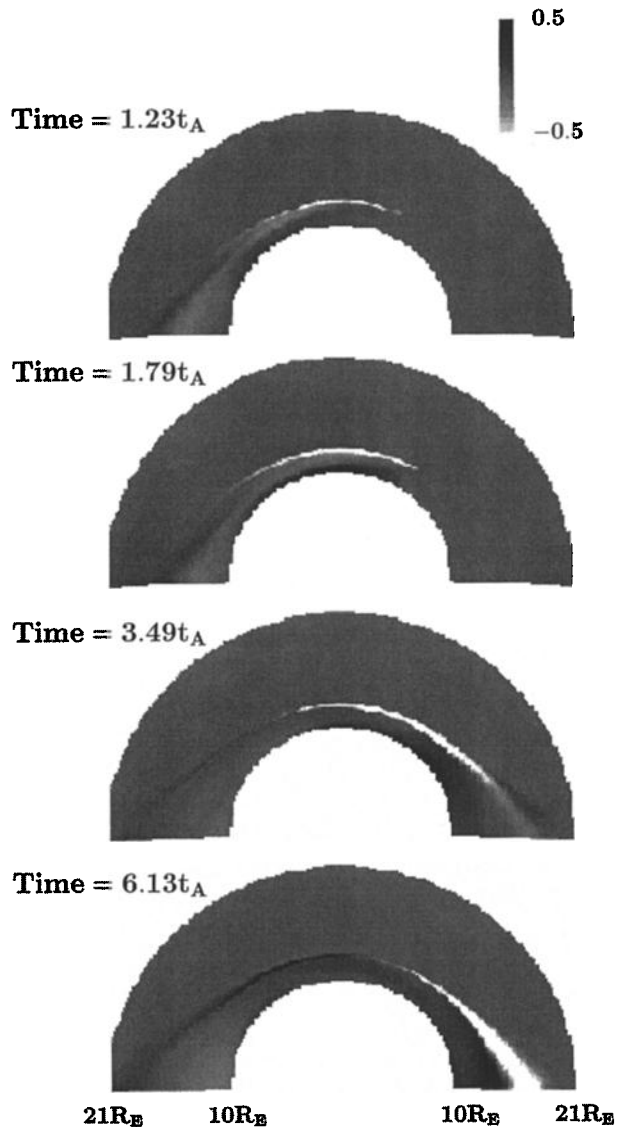
Figure 11. Profiles of several plasma quantities in case 2 along a line running through the dusk ecliptic plane, 45° away from the Sun-Earth line. (a) Density (solid line), thermal pressure (dashed line), and magnetic field magnitude (dotted line) (note that pressure values must be multiplied by 5 and that the scale for magnetic field is given on the right side of the graph). (b) B_x (solid line), B_y (dashed line), and B_z (dotted line). (c) v_x (solid line), v_y (dashed line), and v_z (dotted line). (d) r component of MHD slow wave speed (solid line), r component of MHD intermediate wave speed (dotted line), v_r (dashed line), and r component of MHD fast wave speed (dashed-dotted line). (e) relative change in P_r (solid line) and P_{tot} (dashed line) (P_{tot} has been calculated in a reference frame where the change in dynamic pressure across the RD is zero).

and, after several Alfvén times, advect downstream under the influence of the magnetosheath flow.

It is interesting that the pulse can reach the magnetopause. In order to do so, it must cross the field lines lying above the magnetopause. The original RD, however, being an Alfvén wave, cannot cross field lines. It must be remembered that the standard analysis of MHD waves as slow, intermediate, and fast is of only

limited applicability in the magnetosheath. The magnetosheath's inhomogeneities will produce coupling between these three modes which will allow transfer of energy from one mode to another. So it is conceivable that an RD can give rise to a wave capable of crossing field lines. In fact, such a process would seem to be necessary in the actual magnetosheath, since without it, information of the new upstream solar wind condi-
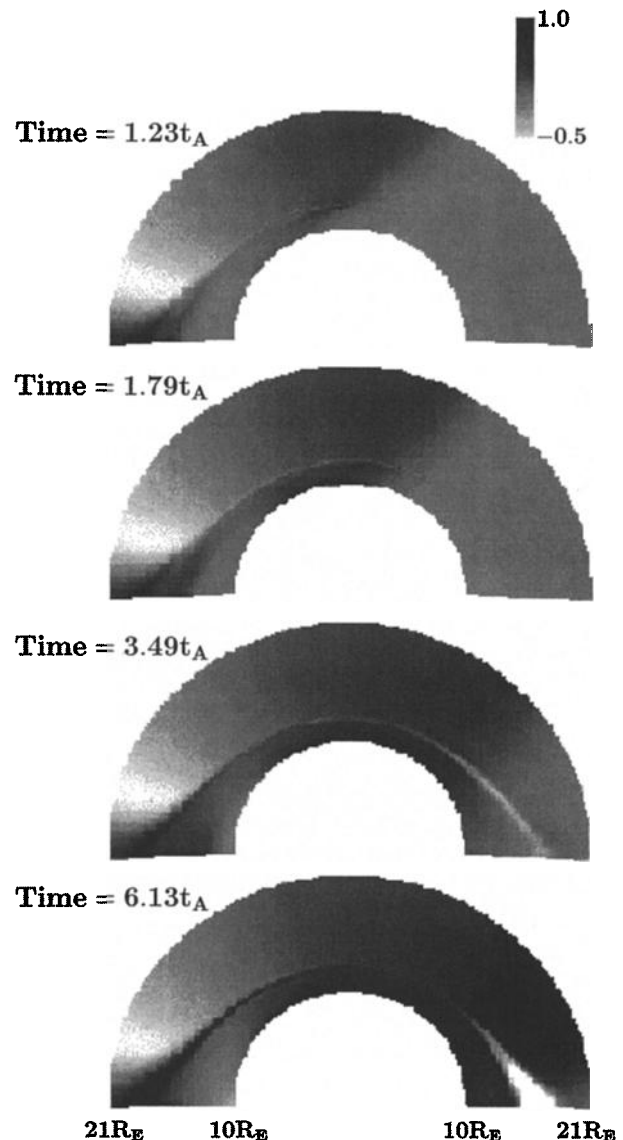
Figure 12. Gray scale plot of relative change in total pressure in the ecliptic plane for the case of the oblique RD at times $t = 1.23t_A$, $1.79t_A$, $3.49t_A$, and $6.13t_A$. Pressures were calculated in a frame of reference where dynamic pressure does not change across the RD, therefore the RD is not seen in the upstream solar wind.

tions behind an RD could never reach the inner magnetosheath and it would never adjust in accordance with the outer magnetosheath and bow shock.

In case 1, the amplitude of the pulse is much stronger in the dawn and subsolar regions than it is in the dusk region. This is probably because of the dawn and subsolar spatial variance in B_x produced by magnetic field line draping. When the pulse contacts the magnetopause, it raises the subsolar and dawn thermal pressures by about 100% and the subsolar and dawn densities by about 75%, but it raises these quantities by only a few percent on the dusk side. P_r rises in the subsolar region by 10% and in the dawn region by close to 100%.

In the dusk region, it drops by 30%. P_{tot} increases by 10% in the subsolar region and 50% in the dawn region. Because of the reference frame in which P_{tot} is calculated, it has a significant temporary increase of 60% on the dusk side.

In case 2, the pulse amplitude is more uniform, though still somewhat larger on the dawn side than on the dusk side. When it contacts the magnetopause, it raises the subsolar density by 37% and thermal pressure by 60%, the dawn density by 40% and thermal pressure by 60%, and the dusk density by 10% and the thermal pressure by 25%. P_{tot} increases by 30% in the subsolar region, 50% on the dawn side, and about 75% on the dusk side. The TDIS character of the pulse is clear on the dusk side, where the increase in pressure clearly occurs with a decrease in magnetic field but is obscured in the subsolar region and on the dawn side. It should be noted

Figure 13. Gray scale plot of relative change in radial pressure in the ecliptic plane for the case of the oblique RD at times $t = 1.23t_A$, $1.79t_A$, $3.49t_A$, and $6.13t_A$.

that though the activity of the pulse is enhanced on the dawn side in both case 1 and case 2, this similarity is coincidental. The enhancement in case 1 is a result of the draping of the unperturbed field lines. The enhancement of case 2 is a result of the alignment of the RD front. If the RD front in case 2 had approached the bow shock from the dawn side instead, everything said here about the dusk and dawn sides in case 2 would be reversed.

One-dimensional MHD and hybrid simulations [Lin et al., 1996a] and 2-D hybrid simulations [Lin et al., 1996b] of rotational discontinuities crossing a fast bow shock have produced strong pressure pulses similar to the ones discussed here. The 3-D simulations represent an advance over the early work in certain respects. First, the inhomogeneities in the 3-D flow cannot be produced in 1-D physics. Also, there is no analogy in 1-D physics to the oblique front case (case 2) and its effect on P_r in particular that we have presented here. Two-dimensional studies can overcome these problems, but their usefulness is still limited. Magnetic flux pileup presents a problem for the 2-D simulations. It forces most bow shocks away from the magnetopause, making it impossible for them to achieve a steady state. Because of flux pileup, the pressure pulse given by Lin et al. [1996b] could not reach the magnetopause. However, had some sort of dissipation been introduced at the magnetopause, it would have artificially affected the pulse's behavior. In our 3-D simulations, a stationary nonparallel bow shock can be produced upstream of a stationary obstacle, and the pressure pulse can be followed all the way to the magnetopause. Further, the 3-D flow produces differences in the behavior of the pulse. Most importantly, as the pulse approaches the magnetopause, its motion slows, and its amplitude increases significantly. Some physics is lost in using MHD simulations instead of hybrid simulations, however. In particular, MHD cannot recover the effects of temperature anisotropy and ion reflection.

With regard to the difference between 1-D and 3-D flow, spreading of the pulse occurred in the 1-D simulations because the leading edge of the pulse was a slow shock propagating in the direction of the plasma flow while the trailing edge was a slow shock propagating opposite the plasma flow. In 3-D, the pulse shows no spread and, in fact, decreases in width as it approaches the magnetopause. The leading edge in 1-D moved with a total velocity of $v_{LE} = v + C_{Sl}$, where v is the flow speed and C_{Sl} is the slow wave speed and the trailing edge moved with a velocity of $v_{TE} = v - C_{Sl}$. In our 3-D simulations, however, v_x and C_{Slx} are significantly smaller at the leading (i.e., Earthward) edge of the pulse than they are at the trailing (i.e., Sunward) edge. So the sum $v_{LE} = v_x + C_{Slx}$ taken at the leading edge does not differ greatly from the difference $v_{TE} = v_x - C_{Slx}$ taken at the trailing edge. Therefore there is no large spread in the pulse. The reflected fast wave we have discussed here could not, of course, appear in 1-D simulations

since, in one dimension, it is impossible to have both a reflective obstacle and a stationary shock. Similar pressure pulses propagating through the magnetosheath have also been produced in the 2-D hybrid simulations of Lin et al. [1996b] and the 2-D MHD simulations of Yan and Lee [1994].

Song et al. [1992] have found slow mode structures in the magnetosheath about 0.4 R_E upstream of the subsolar magnetosphere. It has been suggested that these structures are the slow mode pulses found by Yan and Lee [1994] and now also found in the present 3-D results, consistent with Lin et al. [1996a,b]. Another proposed explanation is that the structures are steady slow shocks or discontinuities generated by the magnetopause-solar wind interaction and serve to further slow the solar wind and deflect it tangential to the magnetopause [Southwood and Kivelson, 1992]. It is hypothesized that such a discontinuity may be necessary in the magnetosheath flow near the magnetopause. The reasoning is that the fast bow shock only slows the plasma flow to a speed below the fast speed, but the component of the flow normal to the magnetopause must be decelerated all the way to zero when the plasma contacts the magnetopause. It would seem then, that the plasma must drop below the slow and intermediate speeds. This would imply the presence of a slow shock.

However, the work shown here indicates that inhomogeneities in the magnetosheath can slow and divert the plasma in the needed manner without creating slow shocks. The component of the plasma velocity normal to the magnetopause must indeed slow to zero. However, note that Figures 3a and 3e in particular, show that the x components of the slow and intermediate speeds normal to the magnetopause also slow to zero. In fact, the three components v_x, C_{Ax}, and C_{Slx} all approach zero in such a way that v_x is always greater than C_{Ax} and C_{Slx}. In other words, the solar wind velocity component normal to the magnetopause drops to zero and yet always remains well above the normal slow and intermediate speeds. Therefore the velocity always remains above the slow and intermediate speeds, and a secondary shock is not necessary. Similarly, Figure 5 shows that in the dusk region, before the approach of the RD, the radial component of velocity is larger than the radial components of the the slow and intermediate speeds at all points from the bow shock to the magnetopause. In contrast, after the RD has passed, the radial velocity is less than the slow and intermediate radial components at all points from the bow shock to the magnetopause. So a slow shock is not necessary in the dusk region either. Similar results are shown for the case of the oblique RD in Figures 9–11. Of course, our results do not categorically rule out the possibility of such a secondary slow shock, but we have demonstrated that such a shock is not always necessary for the diversion of the magnetosheath flow. We conclude that rotational discontinuities may be the source of at

least some of these structures observed by *Song et al.* [1992], but that the issue is still open.

Lin et al. [1996a,b] suggested that MIEs might be caused by the impact of RD-generated pressure pulses on the magnetopause. It is natural to expect that disturbances caused by these pulses will propagate along terrestrial magnetic field lines to the vicinity of the dayside auroral oval. This is indeed where MIEs have been reported [*Lanzerotti et al.*, 1986; *Lanzerotti*, 1989; *Glassmeier et al.*, 1989]. They are also apparently related to changes in the IMF orientation [*Sibeck et al.*, 1989; *Farrugia et al.*, 1989; *Friis-Christensen et al.*, 1988]. This hypothesis is corroborated by the strong pulse impact on the magnetosphere presented here.

A clear link between solar wind RDs and ionospheric MIEs may be established by future simulations that include a freely moving magnetopause and a model of the magnetosphere interior. Such models are necessary to determine how much energy from the pulse can be transmitted into the magnetosphere. We can expect that the pulse will cause oscillations on the magnetopause in a wide range of local times, extending from the Sun-Earth line well into both flanks. The simulations presented here have shown that variations in the IMF direction can produce pressure pulses which may have significant effects on the flanks and in the subsolar region of the magnetopause. With the magnetic field in a typical Parker spiral configuration, the effects on the dawn side can be expected to be particularly large. However, changes in IMF direction, particularly to the south, can also produce FTEs [*Lockwood et al.*, 1989].

References

Cable, S., and Y. Lin, MHD simulations of oppositely propagating Alfvén waves in the magnetosheath and solar wind, *Geophys. Res. Lett.*, *25*, 1821, 1998.

Cable, S., and R.S. Steinolfson, Three-dimensional MHD simulations of the interaction between Venus and the solar wind, *J. Geophys. Res.*, *100*, 21645, 1995.

Farrugia, C.J., M.P. Freeman, S.W.H. Cowley, D.J. Southwood, M. Lockwood, and A. Etemadi, Pressure-driven magnetopause motions and attendant response on the ground, *Planet. Space Sci.*, *37*, 589, 1989.

Friis-Christensen, M., A. McHenry, C.R. Clauer, and S. Vennerstrom, Ionospheric traveling convection vortices observed near the polar cleft: A triggered response to sudden change in the solar wind, *Geophys. Res. Lett.*, *15*, 253, 1988.

Glassmeier, K.-H., and C. Heppner, Traveling magnetospheric convection twin vortices: Another case study, global characteristics, and a model, *J. Geophys. Res.*, *97*, 3977, 1992.

Glassmeier, K.-H., M. Hoenisch, and J. Untiedt, Ground-based and satellite observations of traveling magnetospheric convection twin vortices, *J. Geophys. Res.*, *94*, 2520, 1989.

Konik, R.M., L.J. Lanzerotti, A. Wolfe, C.G. Maclennan, and D. Venkatesan, Cusp latitude magnetic impulse events 2, Interplanetary magnetic field and solar wind conditions, *J. Geophys. Res.*, *99*, 14931, 1994.

Lanzerotti, L.J., Comment on "Solar wind dynamic pressure variations and transient magnetospheric signatures" by D.G. Sibeck, Baumjohann, W., and Lopez, R.E., *Geophys. Res. Lett.*, *16*, 1197, 1989.

Lanzerotti, L.J., L.C. Lee, C.G. Maclennan, A. Wolfe, L.V. Medford, Possible evidence of flux transfer events in the polar ionosphere, *Geophys. Res. Lett.*, *13*, 1089, 1986.

Lapidus, A., A detached shock calculation by second-order finite differences, *J. Comput. Phys.*, *2*, 154, 1967.

Lee, L.C., Magnetic flux transfer at the Earth's magnetopause, in *Proceedings of Chapman Conference on Solar Wind-Magnetosphere Coupling*, edited by Y. Kamide and J. Slavin, p. 297, Terra Sci., Tokyo, 1986.

Lin, Y., L.C. Lee, and M. Yan, Generation of dynamic pressure pulses downstream of the bow shock by variations in the interplanetary magnetic field orientation, *J. Geophys. Res.*, *101*, 479, 1996a.

Lin, Y., D.W. Swift, and L.C. Lee, Simulation of pressure pulses in the bow shock and magnetosheath driven by variations in interplanetary magnetic field direction, *J. Geophys. Res.*, *101*, 27251, 1996b.

Lockwood, M., P.E. Sandholdt, and S.W.H. Cowley, Interplanetary magnetic field control of dayside auroral activity and the transfer of momentum across the dayside magnetopause, *Planet. Space Sci.*, *37*, 1347, 1989.

Lysak, R.L., Y. Song, and D.-H. Lee, Generation of ULF waves by fluctuations in the magnetopause position, in *Solar Wind Sources of Magnetospheric Ultra-Low-Frequency Waves*, Geophys. Monog. Ser. 81, edited by M.J. Engebreston, K. Takahashi, and M. Scholer, p. 273, AGU, Washington, D.C., 1994.

Neubauer, F.M., Nonlinear interaction of discontinuities in the solar wind and the origin of slow shocks, *J. Geophys. Res.*, *81*, 2248, 1976.

Neugebauer, M., D.R. Clay, B.E. Goldstein, B.T. Tsurutani, and R.D. Zwickl, A re-examination of rotational and tangential discontinuities in the solar wind, *J. Geophys. Res.*, *89*, 5395, 1984.

Press, W.H., S.A. Teukolsky, W.T. Vetterling, B.P. Flannery, *Numerical Recipes in FORTRAN*, 963 pp., Cambridge Univ. Press, New York, 1992.

Rubin, E.L., and S.Z. Burstein, Difference methods for the inviscid and viscous equations of a compressible gas, *J. Comput. Phys.*, *2*, 178, 1967.

Saunders, M.A., C.T. Russell, and N. Scopke, Flux transfer events: Scale size and interior structure, *Geophys. Res. Lett.*, *11*, 131, 1984.

Sibeck, D.G., W. Baumjohann, and R.E. Lopez, Solar wind dynamic pressure variations and transient magnetospheric signatures, *Geophys. Res. Lett.*, *16*, 13, 1989.

Sibeck, D.G., K. Takahashi, S. Kokubun, T. Mukai, K.W. Ogilvie, and A. Szabo, A case study of oppositely propagating Alfvénic fluctuations in the solar wind and magnetosheath, *Geophys. Res. Lett.*, 24, 3133, 1997.

Song, P., C.T. Russell, and M.F. Thomsen, Slow mode transition in the frontside magnetosheath, *J. Geophys. Res.*, *97*, 8295, 1992.

Southwood, D.J., Theoretical aspects of ionosphere-magnetosphere solar wind coupling, *Adv. Space Res.*, *5*(4), 7, 1985.

Southwood, D.J., The ionospheric signature of flux transfer events, *J. Geophys. Res.*, *92*, 3207, 1987.

Southwood, D.J., and M.G. Kivelson, The magnetohydrodynamic response of the magnetospheric cavity to changes in solar wind pressure, *J. Geophys. Res.*, *95*, 2301, 1990.

Southwood, D.J., and M.G. Kivelson, On the form of the flow in the magnetosheath, *J. Geophys. Res.*, *97*, 2873, 1992.

Wu, C.C., MHD flow past an obstacle: Large-scale flow in the magnetosheath, *Geophys. Res. Lett.*, *19*, 87, 1992.

Yan, M., and L.C. Lee, Generation of slow-mode waves in front of the dayside magnetopause, *Geophys. Res. Lett.*, *21*, 629, 1994.

S. Cable and Y. Lin, Department of Physics, Auburn University, 206 Allison Lab, Auburn University, Alabama 36849. (e-mail: cablesb@physics.auburn.edu; ylin@physics.auburn.edu)